Morphology of mesoscopic Rh and Pd nanoparticles under oxidizing conditions

F. Mittendorfer, N. Seriani, O. Dubay, and G. Kresse
Computational Materials Physics, Universität Wien, Sensengasse 8/12, A-1090 Vienna, Austria
(Received 9 October 2007; published 28 December 2007)

The thermodynamic equilibrium shape of rhodium and palladium crystals are predicted under conditions from ultrahigh vacuum to high oxygen pressures using the Gibbs-Wulff construction. The analysis is based on data obtained from *ab initio* calculations for the adsorption of oxygen on the low-index (111), (100), and (110) surfaces, and the stepped (311), (211), and (331) surfaces. While the close-packed (111) facets dominate the shape in the low-coverage cases, the higher adsorption energies at the more open surfaces lead to a rounding of the crystallite. A linear correlation between the surface energies of the clean surfaces and the respective adsorption energies is found.

DOI: 10.1103/PhysRevB.76.233413 PACS number(s): 68.43.Bc, 61.46.Hk, 68.65.−k, 82.65.+r

In heterogeneous catalysis, transition metal catalysts are often dispersed as nanoclusters on an oxidic support. Recent studies have demonstrated that for many reactions, the surface orientations present on the crystallite have an impact on the activity of these nanoparticles.[1,2] Therefore, controlling the shape of the nanoparticles is of utmost importance. Although this topic has been extensively investigated in recent decades,[3–10] the conclusions from the experiments are not definitive. The first reason is the so-called "pressure gap": the shape of the particles is strongly influenced by the thermodynamic and chemical conditions employed. Consequently, experimental techniques, which more often than not rely on ultrahigh vacuum, will not be able to capture the relevant cluster morphology under more realistic pressures. The second experimental problem is the difficulty in reaching the equilibrium shape as shown by the wide range of experimentally observed particle shapes.[3–5,7] Nevertheless, regarding the late transition metals Rh and Pd, most experiments lead to the conclusion that predominantly the less active (100) and (111) facets are exposed.

Using the Wulff construction,[11] theoretical methods allow one to predict the morphology of crystals under thermodynamic equilibrium. Only state-of-the-art *ab initio* calculations are accurate enough for realistic predictions. In this Brief Report we present the morphological changes of rhodium and palladium crystallites from UHV to high oxygen pressures assuming thermodynamic equilibrium between the gas phase and the metal surface, as a step towards a systematic understanding of the relation between oxygen pressure and the shape of nanoparticles.

The DFT calculations have been performed using the Vienna *ab initio* simulation package (VASP),[12] using a plane-wave basis set with a cutoff energy of 250 eV, PAW potentials,[13] and the PW91 exchange-correlation functional.[14] The Brillouin zone integration was performed applying Monkhorst-Pack *k*-point meshes with a typical *k*-vector distance of 0.02 $Å^{-1}$. The respective surface orientations were modeled by periodically repeated slabs, consisting of six metal layers for the close-packed (111), eight layers for the more open (100) surface, and ten layers for the (110) surface. For the stepped surfaces six layers parallel to the (111) terraces were used. Unless the superstructure of the adsorbates required larger cells, we used $p(2\times 2)$ supercells for the low-index and $p(2\times 1)$ supercells for the stepped surfaces (doubled along step edge).

The Gibbs free surface energy is calculated as

$$\gamma(\mu_M,\mu_O) = (E_{tot} - N_M\mu_M - N_O\mu_O)/A - \gamma_{bare}(\mu_M), \quad (1)$$

with the total slab energy E_{tot}, the number of metal (oxygen) particles N_M (N_O), and the surface area A. The surface energy of the bare surface, γ_{bare}, is subtracted due to the slab approach used in the calculations (one side bare, second side oxygen covered). The chemical potential of the metal atoms, μ_M, is fixed to the binding energy of the bulk phase, while the gas phase values are used for the chemical potential of oxygen, $\mu_O = 1/2E_B(O_2) + \Delta\mu_O$, neglecting the vibrational contributions of adsorbates and substrate.

At thermodynamic equilibrium, the shape of a freestanding nanoparticle can be found from the Gibbs-Wulff construction.[11] For a particle with facets of areas A_i and corresponding surface energies γ_i, the Gibbs surface free energy G can be written as $G=\Sigma\gamma_i A_i$. The Wulff construction yields the crystal shape that minimizes the free energy G at constant volume and results in a particle shape with a constant ratio between the surface energy γ_i and the distance d_i of the corresponding basal plane to the center of the cluster as follows:

$$\gamma_i/d_i = \text{const.} \quad (2)$$

Since the contributions from the particle edges are neglected in the Wulff construction, the shape of small particles might deviate from the predictions, but experimental analysis indicates that particles in the range of tens of nanometers are generally already consistent with this construction principle.[3,9] On the other hand, due to the mass transport involved, high temperatures or long times might be necessary to reach the equilibrium shape for larger particles. We have applied the Wulff construction taking into account the three low-index surfaces and selected stepped surfaces, namely, (211), (311), and (331). For the bare surfaces, other facets such as (210) and (411) change the general conclusions only a little. We can distinguish four different regimes: the bare surface, the onset of oxygen adsorption, high coverage structures, and surface oxides.

For the bare low- and high-index surfaces of Pd and Rh,

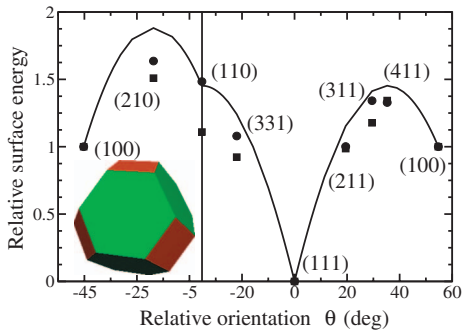

FIG. 1. (Color) Relative surface energies of Rh (squares) and Pd (circles) bare surfaces, and predictions of the bond-breaking model (solid line) (see the text). The surface energies are specified as $[\gamma - \gamma(111)]/[\gamma(100) - \gamma(111)]$.

Fig. 1 shows the relative surface energies. To allow for a straightforward comparison the difference to the (111) surface is scaled by the surface energy difference between the (100) and (111) bare substrate $\gamma(100) - \gamma(111)$. As a reference, results for a simple bond-breaking (BB) model are also shown as a line. In the bond-breaking model, the binding energy is strictly linearly proportional to the total number of bonds, and the model is relevant for the present case, since it predicts that all low-index surfaces, including the (110) facets, are unstable resulting in a capped octahedral shape as shown in the inset of Fig. 1.[15] In the *ab initio* calculations, other surfaces than (100) and (111) can be stable only if the relative surface energy lies below the solid line predicted by the BB model. The present calculations clearly show that this is the case, and the corresponding equilibrium shapes are shown in Fig. 3 (leftmost crystal). In both cases, the (110) surface is predicted to be slightly unstable and is replaced by two (331) facets. The energy difference is, however, so small that one cannot predict with certainty whether the low-index (110) surface is indeed unstable towards faceting. The boundaries between the (100) and (111) facets are not sharp, but intermediate high-index surfaces are readily exposed, with the (311) surface being stable for Rh, and the (211) facet being stable for Pd. Therefore, *Pd and Rh crystals do not expose sharp edges between the low-index surfaces, but high-index surfaces show up between the dominant low-index facets*.

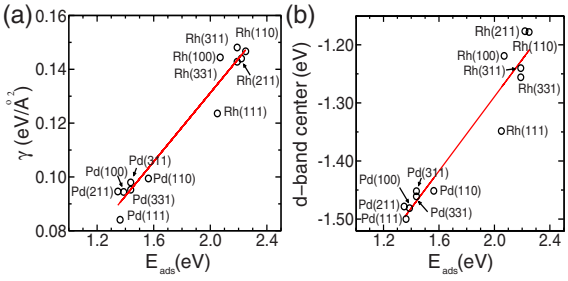

FIG. 2. (Color online) Correlation between low-coverage adsorption energy and (a) surface energy of the bare surfaces and (b) the *d*-band center. Bulk metal *d*-band centers taken from Fig. 10 in Ref. 16, and relative shifts calculated from the local density of states in the surface layer.

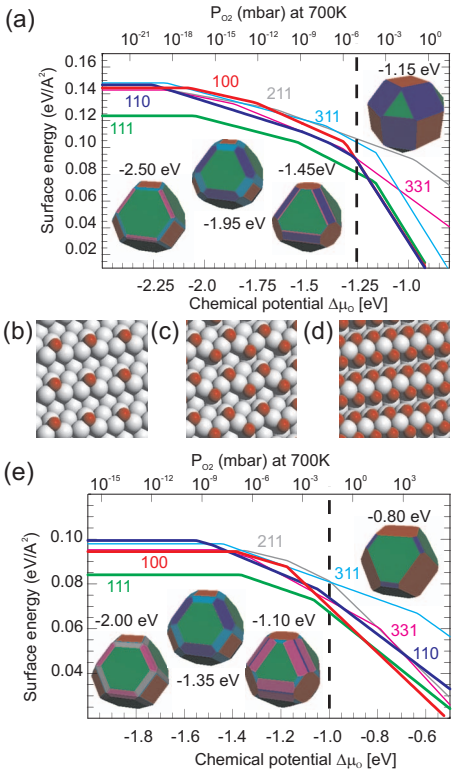

FIG. 3. (Color) (a) Comparative phase diagram of oxygen adsorption on selected Rh and Pd surfaces: [(a) and (e)] (111): green, (100): red, (110): blue, (311): light blue, (211): gray. Stable oxygen adsorption phases on Rh(331) [(b)–(d)]. The vertical lines in the phase diagrams are referring to the stability regime of the bulk oxides.

Concerning the absolute surface energies, we note that the Rh surface energies are much larger than those of the Pd surfaces. For the low-index Rh surfaces we obtain 124 meV/Å^2, 144 and 147 meV/Å^2 for the (111), (100), and (110) facets, respectively, while the corresponding values for the Pd low-index surfaces are 84 meV/A^2, 94 meV/A^2, and 99 meV/A^2. The value for the Rh(100) surface is very close to that of the Rh(110) surface, implying that this surface is less stable than predicted, e.g., by the simple BB model. For low-index Rh surfaces, the relative surface energies [scaled by $\gamma(100) - \gamma(111)$, squares in Fig. 1] are thus lying well below the bond-breaking model. As a consequence, the (100) facets are slightly less pronounced on Rh than on Pd.

As oxygen adsorption sets in, the ratio between the Gibbs free surface energies, and consequently the crystal shape, changes. The close-packed (111) and (100) surfaces gener-

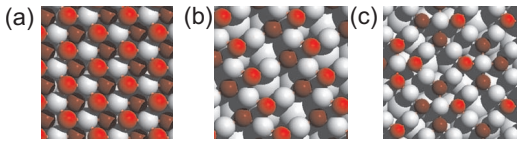

FIG. 4. (Color) Structural models for ultrathin surface oxides on (a) Rh(110), (b) Pd(100), and (c) Pd(111). The oxygen atoms in the topmost layer are displayed in light red, O in the lower layer in dark red, and the metal atoms in gray.

ally yield the lowest adsorption energies (Rh: 2.05 and 2.07 eV/O atom; Pd: 1.36 and 1.39 eV/O atom, respectively), the (110) the largest (Rh: 2.25 eV/O atom, Pd: 1.56 eV/O atom), while stepped surfaces give intermediate values; a systematic evaluation suggests a linear correlation between the low-coverage adsorption energy and the respective surface energy of the bare surface [Fig. 2(a)], with a correlation coefficient of 0.98. Thus in the case of Rh and Pd, the qualitative notion that more open surfaces are more reactive and therefore yield a higher adsorption energy can be expressed in the form of a single quantitative linear relation valid for both metals. Another common descriptor is the *d*-band center, which yields a similar correlation coefficient of 0.96 as shown in Fig. 2(b).[2,16]

As a direct consequence, oxygen adsorption sets in earlier on the open (110) facets. Resultingly, the ratio of the surface energies decreases; first (110) facets appear at the cost of (331) facets, but as oxygen adsorption sets in on the other low-index surfaces, the main effect is that the relative fractions of the (111) and (100) facets shrink, and the crystals tend to become rounder. The crystal shape for oxygen chemical potentials typical of this regime correspond to the second crystal in the insets of Fig. 3(a). It is noted that the Pd and Rh behave remarkably similar at low chemical potentials, roughly 0.2–0.4 eV above the initial adsorption threshold of oxygen.

At higher oxygen coverage, considering and calculating all required oxygen adsorption structures becomes a tedious and cumbersome task. Fortunately, for Rh and Pd, significant data has been acquired in recent years on all closed-packed and few selected high-index surfaces.[17–20] On the close-packed Rh(111) surface, the highest attainable oxygen coverage is 0.5 ML resulting in a (2×1) structure.[17] This structure is also commonly stable on larger (111) terraces. On the (100) facets a $c(2\times2)$ clockwork reconstruction is found.[19] Figures 3(b)–3(d) show, for a prototypical case, how the decoration of step edges proceeds with increasing oxygen partial pressure. Oxygen initially adsorbs on the upper step edge in the threefold hollow site [Fig. 3(b)]. Then the terraces behind the step edge are filled until the (2×1) structure is realized (not shown), and at the same time oxygen adsorption sets in on the lower step edge, leading to a zig-zag decoration of all step edges [Fig. 3(c)]. The edges decorated with a zig-zag pattern repel each other; for instance, a full monolayer of oxygen cannot be realized on the Rh(110) substrate.[18,21] Instead, at higher coverage, two oxygen atoms decorate each step atom symmetrically as shown in Fig. 3(d). The same symmetric oxygen decoration is found on all stepped Rh surfaces we have investigated to date, and the sequence shown in Figs. 3(b)–3(d) is prototypical for surfaces with a high step density including Rh(110).

For Pd the maximal oxygen coverage on the low-index surfaces is 0.25 ML resulting in a $p(2\times2)$ structure, and this is also the typical structure found to be stable on larger terraces. The oxidation of step edges proceeds in a similar manner as for Rh [Figs. 3(b)–3(d)], with the only difference that the final structure, Fig. 3(d), is not stable on Pd. Also the repulsion between oxygen decorated rows is stronger leading to missing-row reconstructions already at rather low oxygen coverage.

The predicted crystal shapes at these intermediate oxygen coverages are also shown in Figs. 3(a) and 3(e) (third crystallite from the left). Although some caution is required since the set of structural models might be incomplete, we find again that the trends are remarkably similar for both metals, although the detailed atomistic structures differ on both metals. One recognizes that the edges between the (100) and (111) facets are now sharp, whereas those between between the (111) facets tend to be round. The explanation is that (i) oxygen decorates the step edges either in a zig-zag pattern or symmetrically, and (ii) oxygen prefers pseudothreefold sites. Step edges between two (111) facets are therefore favorable, whereas those between (111) and (100) facets are energetically not preferred at higher oxygen adsorption, leading to sharp edges between (111) and (100) facets.

Surface oxides form the final regime. On all Rh surfaces, the surface oxide is a 2-Å-thick film consisting of a hexagonal Rh layer sandwiched between two oxygen layers [Fig. 4(a)]. It only sets in just before the stability regime of the bulk oxide, predicted to occur at −1.25 eV.[18,20] Therefore, they are only metastable and might be only observable, if kinetics hinders the formation of a thicker bulklike oxide (which we have not considered in the present work). Attempts to build models for the surface oxides on the stepped surfaces turned out to be illusive, because the O-Rh-O trilayer [Fig. 3(a)] wants to form a two-dimensional noninterrupted closed layer, which cannot be realized on low-index surfaces. Thus stepped surfaces completely vanish at higher oxygen pressure, and are replaced by atomically flat surfaces. On the other hand, the surface energies of the oxide films on the low-index (100), (111), and (110) surface are nearly identical, which leads to a rounded crystal shape dominated by (100) and (110) facets at or beyond a chemical potential of $\mu_O=-1.25$ eV.

For Pd the situation is slightly different, since surface oxides are stable well before the formation of the bulk oxides. They set in at a chemical potential of oxygen of roughly −1.2 eV. The main difference to Rh is that the surface oxides are more dependent on the substrate orientation and show also much stronger bonding to the substrate. The Pd and O atoms are now coplanar with a buckling of 0.6 Å in the oxygen plane. Stable surface oxide layers have been observed on Pd(100) (Fig. 3, red line),[22] Pd(111) (Fig. 3, green line),[23–27] but not for Pd(110), which we found confirmed by theoretical calculations. As a result, the surface energies for the (100) and (111) facets are close, whereas only minor contributions of the (110) facet are exposed. A common trend with the Rh surface is that, if surface oxides form, they essentially level the surface energies.

We now briefly turn to a comparison with experiment. In fact, reliable data are remarkably scarce for transition metals, and we are only aware of studies of supported Pd nanoparticles.[8,28] Our calculations predict an anisotropy ratio $\gamma_{100}/\gamma_{111}$ of 1.12 for the bare surfaces, which nicely corresponds to the value of 1.16 estimated from the shape of nanoparticles annealed under UHV conditions.[8] At higher oxygen pressure, however, our data deviate significantly from the measured ones: at an oxygen pressure of 10^{-3} Torr (1.3×10^{-6} bars) and a temperature of 550 °C, corresponding to a chemical potential of $\mu_O=-1.32$ eV, the value esti-

mated from experimental measurements is 0.72,[8] while our calculations predict a strong drop in the ratio only in the stability regime of the surface oxides. Presumably this discrepancy is due to the kinetical suppression of oxide formation in the experiments.

In summary, in accordance with the commonly accepted picture that atomically flat surfaces will dominate the surfaces of nanocrystals, the (111) and (100) facets are found to be most stable at low pressures. But our results predict that Rh and Pd crystals also expose a noticeable fraction of low index, stepped surfaces [(311), (211), and (331) facets] under UHV conditions. Such a prediction cannot be derived from a simple BB model.[15,29] Although stepped surfaces had already been predicted to be stable for Cu (Ref. 30) and Pb crystals,[31,32] our present calculations for transition metals are particularly relevant since Rh and Pd are among the most important catalytically active metals.[33] The situation does not change appreciably at intermediate pressures, i.e., the already mentioned low-index surfaces remain relevant. Actually, the higher oxygen pressure tends to reduce the differences in the surface energies yielding rounder crystals with more atomically rough surfaces at higher pressures. This is related to a linear relationship between oxygen adsorption energies and surface energies. Therefore, oxygen adsorption sets in earlier on the originally less stable, more open surfaces, in particular (110), counteracting their inherent instability under UHV conditions. This shows that the study of low-index surfaces might in no way suffice to establish a full picture of the catalytic properties of nanocrystals. The situation changes again at very high oxygen pressures, at which surface oxide formation takes place. Under these conditions only the flat low-index facets show up at the crystallite surfaces, with relative areas strongly differing from those under UHV conditions. This clearly shows that the interplay between pressure and crystal shape is complex and deserves much further work.

This project was supported by Austrian Science Fund (FWF) and the European Union under Contract No. NMP3-CT-2003-505670 (NANO2).

[1] B. K. Hodnett, *Heterogeneous Catalytic Oxidation* (John Wiley & Sons Ltd., Chichester, UK, 2000).
[2] J. K. Nørskov, T. Bligaard, A. Logadottir, S. Bahn, L. B. Hansen, M. Bollinger, H. Bengaard, B. Hammer, Z. Sljivancanin, M. Mavrikakis, Y. Xu, S. Dahl, and C. J. H. Jacobsen, J. Catal. **209**, 275 (2002).
[3] L. D. Marks, Rep. Prog. Phys. **57**, 603 (1994).
[4] F. Silly and M. R. Castell, Phys. Rev. Lett. **94**, 046103 (2005).
[5] J. D. Hoefelmeyer, K. Niesz, G. A. Somorjai, and T. D. Tilley, Nano Lett. **5**, 435 (2005).
[6] K. Hojrup Hansen, T. Worren, S. Stempel, E. Laegsgaard, M. Bäumer, H.-J. Freund, F. Besenbacher, and I. Stensgaard, Phys. Rev. Lett. **83**, 4120 (1999).
[7] C. Chapon, S. Granjeaud, A. Humbert, and C. R. Henry, Eur. Phys. J.: Appl. Phys. **13**, 23 (2001).
[8] H. Graoui, S. Giorgio, and C. R. Henry, Surf. Sci. **417**, 350 (1998).
[9] H. Graoui, S. Giorgio, and C. R. Henry, Philos. Mag. **81**, 1649 (2001).
[10] N. Kasper, A. Stierle, P. Nolte, Y. Jin-Phillipp, T. Wagner, D. G. de Oteyza, and H. Dosch, Surf. Sci. **600**, 2860 (2006).
[11] G. Wulff, Z. Kristallogr. **34**, 445 (1901).
[12] G. Kresse and J. Hafner, Phys. Rev. B **47**, 558 (1993).
[13] G. Kresse and D. Joubert, Phys. Rev. B **59**, 1758 (1999).
[14] J. P. Perdew, J. A. Chevary, S. H. Vosko, K. A. Jackson, M. R. Pederson, D. J. Singh, and C. Fiolhais, Phys. Rev. B **46**, 6671 (1992).
[15] J. W. M. Frenken and P. Stoltze, Phys. Rev. Lett. **82**, 3500 (1999).
[16] B. Hammer and J. K. Nørskov, Adv. Catal. **45**, 71 (2000).
[17] L. Köhler, G. Kresse, M. Schmid, E. Lundgren, J. Gustafson, A. Mikkelsen, M. Borg, J. Yuhara, J. N. Andersen, M. Marsman, and P. Varga, Phys. Rev. Lett. **93**, 266103 (2004).
[18] C. Dri, C. Africh, F. Esch, G. Comelli, O. Dubay, L. Khler, F. Mittendorfer, G. Kresse, P. Dudin, and M. Kiskinova, J. Chem. Phys. **125**, 094701 (2006).
[19] J. Gustafson, A. Mikkelsen, M. Borg, J. N. Anderson, E. Lundgren, C. Klein, W. Hofer, M. Schmid, P. Varga, L. Köhler, G. Kresse, N. Kasper, A. Stierle, and H. Dosch, Phys. Rev. B **71**, 115442 (2005).
[20] E. Lundgren, A. Mikkelsen, J. N. Andersen, G. Kresse, Michael Schmid, and Peter Varga, J. Phys.: Condens. Matter **18**, R481 (2006).
[21] J. Gustafson, A. Resta, A. Mikkelsen, R. Westerström, J. N. Andersen, E. Lundgren, J. Weissenrieder, M. Schmid, P. Varga, N. Kasper, X. Torrelles, S. Ferrer, F. Mittendorfer, and G. Kresse, Phys. Rev. B **74**, 035401 (2006).
[22] J. Rogal, K. Reuter, and M. Scheffler, Phys. Rev. Lett. **98**, 046101 (2007).
[23] E. Lundgren, G. Kresse, C. Klein, M. Borg, J. N. Andersen, M. De Santis, Y. Gauthier, C. Konvicka, M. Schmid, and P. Varga, Phys. Rev. Lett. **88**, 246103 (2002).
[24] D. T. Vu, K. A. R. Mitchell, O. L. Warren, and P. A. Thiel, Surf. Sci. **318**, 129 (1994).
[25] M. Todorova, E. Lundgren, V. Blum, A. Mikkelsen, S. Gray, J. Gustafson, M. Borg, J. Rogal, K. Reuter, J. N. Andersen, and M. Scheffler, Surf. Sci. **541**, 101 (2003).
[26] A. I. Titkov, A. N. Salanov, S. V. Koscheev, and A. I. Boronin, Surf. Sci. **600**, 4119 (2006).
[27] P. Kostelník, N. Seriani, G. Kresse, A. Mikkelsen, E. Lundgren, V. Blum, T. Sikola, P. Varga, and M. Schmid, Surf. Sci. **601**, 1574 (2007).
[28] T. Schalow, B. Brandt, D. E. Starr, M. Laurin, S. Schauermann, Sh. K. Shaikhutdinov, J. Libuda, and H.-J. Freund, Catal. Lett. **107**, 189 (2006).
[29] M. C. Desjonquères, D. Spanjaard, C. Barreteau, and F. Raouafi, Phys. Rev. Lett. **88**, 056104 (2002).
[30] J. L. F. Da Silva, C. Barreteau, K. Schroeder, and S. Blügel, Phys. Rev. B **73**, 125402 (2006).
[31] D. K. Yu, H. P. Bonzel, and M. Scheffler, Phys. Rev. B **74**, 115408 (2006).
[32] D. K. Yu, H. P. Bonzel, and M. Scheffler, New J. Phys. **8**, 65 (2006).
[33] M. Mavrikakis, M. Bäumer, H.-J. Freund, and J. K. Nørskov, Catal. Lett. **81**, 153 (2002).